JOURNAL OF GUIDANCE, CONTROL, AND DYNAMICS
Vol. 25, No. 2, March–April 2002

Reduced-Order Entry Trajectory Planning for Acceleration Guidance

K. D. Mease,* D. T. Chen,† P. Teufel,‡ and H. Schönenberger§
University of California, Irvine, California 92697

The acceleration guidance concept is to plan an aerodynamic acceleration profile that integrates to the desired final position and velocity and satisfies all vehicle constraints and to track the acceleration profile. The longitudinal entry guidance for the space shuttle is acceleration guidance; a drag deceleration profile that integrates to the desired downrange and satisfies the vehicle constraints is planned and tracked primarily by bank-angle adjustments. The kinematics relating the drag profile to the downrange assume that the entry trajectory is a great circle arc. In this paper we consider lateral as well as longitudinal motion in acceleration planning. Three differential equations that are the kinematic relations between the aerodynamic accelerations and the position and velocity variables with energy as the independent variable are used as the basis for two methods of planning the drag and lateral acceleration profiles. The first is simpler and produces a feasible trajectory for a given angle-of-attack profile. The second requires more computation, but produces an optimal trajectory using both angle-of-attack and angle-of-bank variations to control the entry trajectory and has greater capability to shape the entry trajectory. Both methods are demonstrated using an X-33 vehicle model. The optimal method is capable of achieving a specified final heading angle and adjusting the number of bank reversals.

Introduction

THE entry guidance method used by Space Shuttle Orbiter has proven effective for the current space transportation system and was selected as the baseline method for the next generation reusable launch vehicle (RLV) technology demonstrators: X-33,[1] X-34, and X-37. Our purpose in this paper is to extend this method to allow greater entry capability for future RLVs. Other promising approaches[2–6] have also been developed since the space shuttle entry guidance.

Experience in entry vehicle guidance prior to the space shuttle led to the conclusion[7] that entry guidance schemes should be centered on aerodynamic acceleration. Aerodynamic acceleration can be accurately measured and translated into position and velocity via kinematic relations. Predictive guidance schemes that rely too heavily on knowing how the angles of attack and bank translate into aerodynamic accelerations are not sufficiently robust. For example the Gemini entry guidance commanded the bank angle required to reach the landing target based on force modeling and prediction; the actual lift-to-drag ratio (L/D) of Gemini III was 35% lower than the predicted value, which was a significant contributor to the 60-n mile landing error.[7] Although aerodynamic force modeling is more accurate today, it continues to be a significant source of error with which guidance schemes must contend.

The entry guidance algorithms for Apollo (excluding the initial skip out and reentry maneuver for extending range, which was never used) and the precision recovery including maneuvering entry vehicle were based on tracking a stored drag acceleration profile to control downrange. Acceleration guidance proved to be robust to L/D variations and many other errors. The longitudinal portion of the space shuttle entry guidance[8] is acceleration guidance, with the important added capability of replanning the drag acceleration profile during flight to null the predicted downrange error. Wingrove[9] provides a useful overview of acceleration and other entry guidance approaches. More recently there have been several[10–14] extensions and applications of drag acceleration guidance.

One means of controlling the flight path of an unpowered lifting entry vehicle is to adjust the bank angle and thus control the direction of the lift vector. The drag acceleration is controlled by the vertical component of the lift.[9] For a given angle of attack, the vertical component of lift dictates the lateral component of lift, except for the sign of this component. Whenever the lift vector has a nonzero lateral component, the direction of the lateral component—right or left—can be chosen to reduce the heading error. In addition to acceleration guidance for downrange, the shuttle guidance includes a cross-range logic for commanding the sign of the lateral component of lift, or equivalently the sign of the bank angle.

The shuttle entry guidance has been very effective; however, the next generation of RLVs and orbital transfer vehicles would benefit from a greater level of autonomy and capability relative to that of the shuttle. Our objective in this paper is to develop a more capable entry trajectory planning method that would be applicable to large cross-range entries and onboard abort planning. Our approach is to extend the planning portion of the shuttle entry guidance while retaining its attributes. In particular, we will consider lateral motion as well as the longitudinal motion and not assume, in contrast to the shuttle planning, that the entry trajectory is a great circle arc. We note that these developments are not necessary for effectively guiding the nominal shuttle entry because the feasible landing footprint for the shuttle is sufficiently restrictive relative to the footprint dictated by its maneuvering capability alone because of a variety of additional constraints. For the Hermes spaceplane, which needed to use much of its cross-range capability without sacrificing accuracy, the space shuttle-type entry guidance was judged[15] inadequate. The proposed scheme was to compute a reference trajectory prior to flight, store the corresponding aerodynamic acceleration profiles onboard, and use a feedback law to track the accelerations. For entry the drag and lateral accelerations corresponding to the reference trajectory were tracked by commanding both angle of attack and angle of bank. Simulations showed this scheme to be effective; however, the fact that it is based on a precomputed reference trajectory limits its autonomy and adaptivity. For next generation RLVs enhanced onboard entry planning capability would be a beneficial step toward the often stated goal of more aircraft-like operations.

In this paper we present two methods for planning both the drag and lateral accelerations. The methods are based on a reduced-order

Received 1 December 2000; revision received 16 August 2001; accepted for publication 21 August 2001.

*Professor, Department of Mechanical and Aerospace Engineering. Associate Fellow AIAA.

†Graduate Research Assistant, Department of Mechanical and Aerospace Engineering.

‡Visiting Student, Department of Mechanical and Aerospace Engineering; currently Graduate Research Assistant, Institute for Flight Mechanics and Control, University of Stuttgart, Germany.

§Visiting Student, Department of Mechanical and Aerospace Engineering; also Student, University of Stuttgart.

model. The methods are natural extensions of the drag planning technique used in the space shuttle guidance. The first method assumes an angle-of-attack profile, as in the shuttle entry planning, and produces a feasible trajectory. It starts with drag acceleration planning based on the great circle arc approximation, but then successively refines the drag and lateral accelerations to account for the trajectory curvature in the lateral direction. The second method requires more computation, but produces an optimal trajectory and offers more flexibility. In the second method an adjustable angle of attack is assumed. For an entry vehicle with an adjustable trim angle of attack, it is possible to independently adjust the vertical and lateral components of lift within certain limits, thus offering more freedom in controlling the trajectory. The space shuttle does use angle-of-attack modulation as a supplementary trajectory control mechanism, but this independent means of trajectory control is not considered in the acceleration planning.

Entry Planning Problem

Entry Dynamics

The state space for the translational motion (i.e., the position-velocity space) is six-dimensional. Because we will model the entry dynamics as time independent, we can consider five state variables to be functions of a sixth state variable if this sixth state variable is strictly monotonic along the trajectories of interest. We shall consider five state variables as functions of the strictly decreasing energy E defined by

$$E = \tfrac{1}{2}V^2 - (\mu/r - \mu/r_s) \tag{1}$$

where V is the Earth-relative velocity magnitude; r and r_s are the radial distances from the planet center to the vehicle center of mass and the planet surface, respectively; and μ is the gravitational constant. This is an appropriate formulation[2] for the entry problem because the terminal conditions are given at an energy value, whereas time plays no role. The formulation does require that the trajectory segment under consideration has a consistently decreasing energy. For an entry trajectory the initial state must be specified at a point where the drag has become significant.

Denoting $\mathrm{d}(\cdot)/\mathrm{d}E$ by $(\cdot)'$, using $(\cdot)' = (1/\dot{E})\,\mathrm{d}(\cdot)/\mathrm{d}t$ and $\dot{E} = -\mathrm{D}V$, ignoring the coriolis and centripetal accelerations caused by rotation and neglecting winds, the translational equations of motion[16] for the center of mass of an unpowered vehicle of constant mass take the form

$$\theta' = -\frac{\cos\gamma\cos\psi}{r\cos\phi}\left(\frac{1}{D}\right), \qquad \phi' = -\frac{\cos\gamma\sin\psi}{r}\left(\frac{1}{D}\right)$$

$$\psi' = \frac{\cos\gamma\cos\psi\tan\phi}{r}\left(\frac{1}{D}\right) + \frac{1}{V^2\cos\gamma}\left(\frac{L}{D}\sin\sigma\right)$$

$$r' = -\sin\gamma\left(\frac{1}{D}\right)$$

$$\gamma' = \left(g - \frac{V^2}{r}\right)\frac{\cos\gamma}{V^2}\left(\frac{1}{D}\right) - \frac{1}{V^2}\left(\frac{L}{D}\cos\sigma\right) \tag{2}$$

where θ is the longitude, ϕ is the latitude, γ is the flight-path angle, and ψ is the heading angle with $\psi = 0$ radians corresponding to flight due east and $\psi = \pi/2$ radians corresponding to flight due north. In these equations V^2 should be interpreted as a function of E and r, specifically, $V^2 = 2[E + (\mu/r - \mu/r_s)]$. Because the velocity V can be determined from r and E, only five equations are necessary. The bank angle σ is defined such that the lift vector is in the vertical plane at zero bank angle and positive bank angle corresponds to banking to the right. The acceleration from gravity is $g = \mu/r^2$. L and D represent the lift and drag accelerations (specific forces) and are given by

$$L = \tfrac{1}{2}\rho(r)V^2 \cdot S/m \cdot C_L[\alpha, M(E,r)]$$

$$D = \tfrac{1}{2}\rho(r)V^2 \cdot S/m \cdot C_D[\alpha, M(E,r)] \tag{3}$$

where $\rho(r)$ is the density as a function of the radial distance r; C_L and C_D are the lift and drag coefficients, which depend on the angle of attack α and Mach number $M(E, r)$; S is the reference area; and m is the vehicle mass. In performing computations it is advantageous to express r in units of r_s; g, D, and L in units of $g_s = \mu/r_s^2$; and E in units of μ/r_s. Because these are consistent units, no change in the equations of motion [Eqs. (2)] are required.

The Coriolis and centripetal acceleration terms could be included in Eqs. (2). Given specific accuracy requirements, an error analysis would determine whether either or both of these terms are required. One advantage to not including them is that it allows us to redefine our coordinates in a more convenient way (see Coordinate Redefinition subsection). Our basic approach is applicable however even if these terms are included.

Vehicle and Control Constraints

The vehicle constraints on the maximum dynamic pressure, aerodynamic acceleration, and heating rate are given by

$$q = \tfrac{1}{2}\rho V^2 \le q_{\max}$$

$$A = (D^2 + L^2)^{\frac{1}{2}} = D[1 + (L/D)^2]^{\frac{1}{2}} \le A_{\max}$$

$$\dot{Q} = c\sqrt{\rho}V^k \le \dot{Q}_{\max} \tag{4}$$

where $k = 3.15$ is used for the numerical results presented later. In the full-order state formulation we are discussing, the angle-of-attack α and the angle-of-bank σ are taken to be the controls. There may be restrictions on the values of both controls. In this paper we only consider energy-dependent bounds on α; namely, we require that $\alpha(E) \in [\alpha_{\min}(E), \alpha_{\max}(E)]$.

Problem Statement

To simplify notation, let $x = (\theta, \phi, \psi, r, \gamma)$ denote the state. The entry dynamics are expressed concisely as $x' = f(x, \alpha, \sigma)$. The target longitude θ_f and latitude ϕ_f are given at a specified final energy E_f; these specifications are represented as terminal equality constraints $\Gamma[x(E_f)] = [\theta(E_f) - \theta_f, \phi(E_f) - \phi_f]^T = (0, 0)^T$. There is typically an allowable interval of final altitudes. Our trajectory planning approach addresses this requirement indirectly, but we do not include this requirement in our problem statement.

The entry trajectory planning problem is as follows: given the state $x(E_0)$ at an initial energy E_0, the terminal constraints and the vehicle constraints, determine feasible controls $[\alpha(E), \sigma(E)]$ on the interval $[E_0, E_f]$. Feasible means that the state trajectory and the controls satisfy the boundary conditions and the vehicle and control constraints.

Existence and Uniqueness of a Solution

For each initial condition there is a five-dimensional reachable set $\mathcal{R}[E_f; x(E_0)]$ of terminal states contained in the five-dimensional terminal energy slice, defined by $E = E_f$, of the six-dimensional state space. The terminal conditions are two independent constraints on the final state and define a three-dimensional terminal manifold in the terminal energy slice of the state space. If the intersection of the terminal manifold and the reachable set is empty, then there is no solution to the entry problem. If the intersection is nonempty, then a solution exists. In this case the solution typically will not be unique, unless the intersection is a single point on the boundary of the reachable set, for instance, the maximum range solution.

Solution Quality

In cases where there are multiple solutions to the entry problem, there are desirable solution qualities that can be used to distinguish and choose between them. The rates and accelerations of the angles of attack and bank should not be too high. The trajectory should not have rapid changes in altitude and speed; these rapid changes are avoided if γ' is small, that is, by flying in near-equilibrium glide. The final heading angle should be compatible with the needs of the TAEM phase guidance. The trajectory and controls should have sufficient margins from the constraint boundaries to allow for dispersions. There are also control authority and further heating considerations that are addressed next.

At each energy and each magnitude of the bank angle, there is a minimum vertical component of lift

$$(L\cos\sigma)_{\min} = g - V^2/r \tag{5}$$

dictated by the equilibrium glide boundary; below this minimum vertical lift the vehicle cannot generate enough lift force to balance the effective weight. For each value of α, there is a maximum altitude that corresponds to the equilibrium glide boundary. The vehicle does not have enough control authority to sustain level flight above this altitude, although transient excursions are possible. By staying within the equilibrium glide boundary, there is excess vertical lift capability for trajectory control. In the case of supercircular speed, it would be necessary to consider bank angles satisfying $(g - V^2/r) < 0$ and $|\sigma| > \pi/2$ radians.

It may be desirable to minimize the heat load

$$Q = \int_{E_0}^{E_f} \dot{Q}\left(\frac{\mathrm{d}E}{\mathrm{d}t}\right)^{-1} \mathrm{d}E \tag{6}$$

depending on the type of thermal protection used for the vehicle. Minimizing the heat load is accomplished by flying on the active vehicle constraint boundary—dynamic pressure, heating rate, or aerodynamic acceleration—for much of the trajectory, which shortens the flight time.[13]

Coordinate Redefinition

Because we are not accounting for planet rotation, the "equatorial" plane can be defined as any plane containing the planet center without having to change the equations of motion. For trajectory planning when the initial and target positions are given, it is convenient to define the equatorial plane as the plane containing the initial position of the vehicle (more precisely the center of mass position) and the target position. The "north pole" is directed such that the shortest path to the target is in the easterly direction. Henceforth, we shall refer to this plane as the target plane. The initial and target positions will always have $\phi = 0$, which is the equation for the target plane. The corresponding heading angle is measured from the direction corresponding to "east" in this target coordinate frame.

Space Shuttle Drag Acceleration Planning

The space shuttle atmospheric descent is divided into three phases: hypersonic entry, terminal area energy management (TAEM), and approach and landing. The hypersonic entry guidance targets to a desired TAEM interface condition; this condition is specified by a longitude, latitude, altitude, and speed. The specified speed is about Mach 2. (What we are calling the hypersonic entry phase includes some supersonic flight.)

The onboard trajectory planning[8] for the shuttle assumes that the hypersonic portion of the entry trajectory is a great circle arc extending from the radial line containing the initial or current vehicle position to the radial line containing the desired TAEM interface position. The radial distance (from the Earth center) corresponding to the TAEM interface altitude, denoted by r_f, is the assumed radius of the great circle arc. The great circle arc is depicted by the dashed line in Fig. 1. In general, the length S of a trajectory is given by

$$S = \int_0^{t_f} V\,\mathrm{d}t = -\int_{E_0}^{E_f} \frac{\mathrm{d}E}{D(E)} = -\int_{V_0}^{V_f} \frac{V\,\mathrm{d}V}{D + g\sin\gamma} \tag{7}$$

With the required trajectory length given by the great circle arc approximation, a drag acceleration profile is specified that is consistent with this trajectory length. By representing $D(E)$ as a piecewise quadratic function of E, the shuttle trajectory planning is done analytically. (For most of the drag segments V rather than E is used as the independent variable in the shuttle formulation. Because $\gamma = 0$ for the assumed great circle arc, the relation between trajectory length and drag is equally simple for the two choices of independent variable. For flight paths for which $g\sin\gamma$ is not negligible compared to D, the independent variable E is preferred.)

In terms of Eqs. (2), the shuttle planning can be viewed as follows. The great circle arc assumption used for the shuttle corresponds

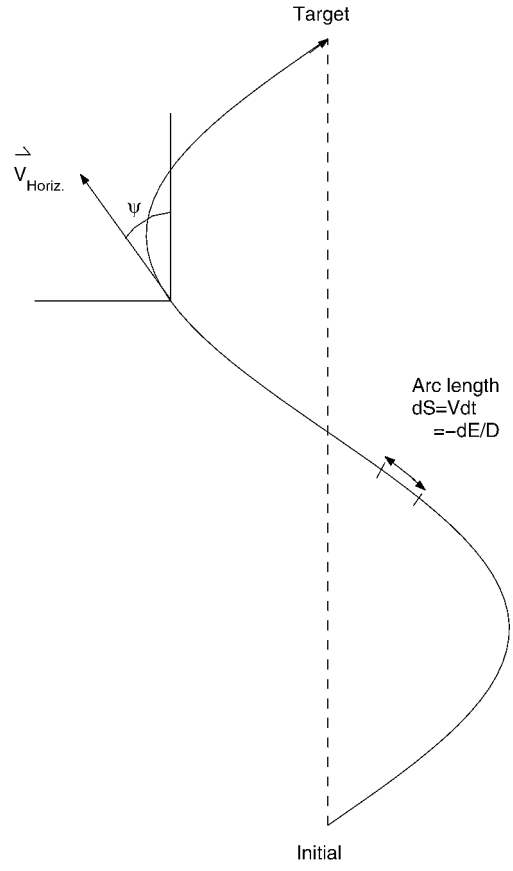

Fig. 1 Projection of flight path onto constant altitude surface illustrating the trajectory length and curvature subproblems.

to the conditions $\psi = 0$, $\phi = 0$, $\cos\gamma = 1$, and $r = r_f$. Under these conditions the first equation of Eqs. (2) reduces to

$$\theta' = -(1/r_f)(1/D) \tag{8}$$

θ is then the angular displacement along the great circle arc or one can use distance variable $R = r_f\theta$. Equation (8) is the differential form of the integral equation (7).

Flying an arbitrary drag acceleration profile may cause violations of the constraints. Fortunately, the vehicle constraints can all be represented as drag acceleration constraints. An entry corridor can be plotted in the drag vs energy plane. At each energy there is a maximum drag dictated by the active vehicle constraint. There is also a minimum drag corresponding to the minimum lift dictated by the zero bank equilibrium glide condition

$$L_{\min} = g - V^2/r \tag{9}$$

We limit our attention here to the subcircular case for which $(g - V^2/r) > 0$. The shuttle trajectory planning assumes a fixed angle-of-attack profile. With α given as a function of E and $r = r_f$, there is a unique value of L/D for each value of E. Thus we have

$$D_{\min} = L_{\min}(L/D)^{-1} = (g - V^2/r)(L/D)^{-1} \tag{10}$$

If D is less than $D_{\min}$, there is insufficient lift to achieve either $\gamma' < 0$ or (i.e., $\dot{\gamma} > 0$), indicating a lack of maneuverability. By selecting a drag profile that lies within the entry corridor, satisfaction of the vehicle constraints and maneuverability to accommodate dispersions are ensured. An acceptable heat load is achieved by biasing the drag profile toward the maximum drag boundary as discussed earlier.

Once the drag profile has been determined, the other trajectory and control information, consistent with this drag profile, can be computed. The first and second derivatives of the drag acceleration with respect to energy provide algebraic relations satisfied by the state and control variables. At each energy, with the angle of attack given, r can be extracted from the drag model; in general, the

extracted r will not be r_f. The D' and D'' equations can then be solved for γ and $(L/D)\cos\sigma$. In this manner a complete longitudinal reference trajectory is prescribed in the target plane.

The reference trajectory is tracked in the longitudinal plane by tracking the reference drag profile. For tracking, $(L/D)\cos\sigma$ is viewed as the commanded variable; bank angle modulation is the primary means of achieving the command, but α adjustment is used as a secondary means. In general, flying the planned drag acceleration profile will require $|(L/D)\cos\sigma| < L/D$, that is, the lift vector will be directed out of the vertical plane; hence, $(L/D)\sin\sigma \neq 0$, and the heading angle will change. Furthermore, the initial (or current) heading angle may not be zero as assumed. Consequently, there will typically be lateral motion and ϕ will not be zero. The shuttle guidance handles this lateral motion by defining an azimuth corridor centered on the direction to the target and commanding a bank reversal when a boundary of this corridor is reached. Handling the lateral motion in this manner, while neglecting it in the planning, is a viable guidance approach for the shuttle because its cross ranging is limited by constraints. In the following, we develop a planning procedure that allows for entry trajectories with significant lateral motion.

Combined Drag and Lateral Acceleration Planning

The direct extension of the space shuttle planning to consider lateral motion starts with the assumption that the hypersonic entry flight path evolves on the surface of a sphere, with center coinciding with the Earth's center. Let the radius of the sphere be given by $\hat{r}$. At a minimum we would need to employ the differential equations for longitude and latitude to plan the motion on this sphere. In addition to drag, we could treat the heading angle ψ as a variable to be specified. However, it is not clear what values of ψ would lead to a feasible entry trajectory. Also ψ is not an acceleration and thus does not conform to the acceleration guidance concept. By including the differential equation for the heading angle, we can instead treat the lateral acceleration $L\sin\sigma$ as the second variable to be specified. Although conceptually we view the drag and lateral acceleration components of the total aerodynamic acceleration (or specific force) as the variables we plan, the ratio of the lateral and drag accelerations $[(L/D)\sin\sigma]$ is a little more convenient than $L\sin\sigma$, and we shall use it.

Reduced-Order System

The reduced-order system for trajectory planning is

$$\theta' = -\frac{\cos\psi}{\hat{r}\cos\phi}\left(\frac{1}{D}\right), \qquad \phi' = -\frac{\sin\psi}{\hat{r}}\left(\frac{1}{D}\right)$$

$$\psi' = +\frac{1}{V^2}\left(\frac{L\sin\sigma}{D}\right) + \frac{\cos\psi\tan\phi}{\hat{r}}\left(\frac{1}{D}\right) \tag{11}$$

Although we used flight on the surface of a fixed radius sphere to motivate our approach, we introduce an additional degree of flexibility by specifying $\hat{r}$ as a function of E, not necessarily constant. We do assume that the flight-path angle is sufficiently small that setting $\cos\gamma = 1$ causes a negligible error. The approximations $r = \hat{r}$ and $\cos\gamma = 1$ are only used when evaluating θ', ϕ', and ψ'. We have implicitly defined the small parameter $\epsilon = (r - \hat{r})/\hat{r}$, employed the expansions $r^{-1} = \hat{r}^{-1}(1 + \epsilon + \cdots)$ and $\cos\gamma = 1 - \gamma^2/2 + \cdots$, and neglected the $\mathcal{O}(\epsilon, \gamma^2)$ terms in the differential equations for θ, ϕ, and ψ. Compared to the accuracy with which the drag and lateral accelerations can be measured and tracked, the $\mathcal{O}(\epsilon, \gamma^2)$ terms are negligible. Once θ, ϕ, ψ, D, and $(L/D)\sin\sigma$ are determined, an extraction algorithm described later can be used to determine the corresponding values of r, γ, α, and σ. The extracted values of r and γ in general will not be $\hat{r}$ and 0, respectively.

Equations (11) are the kinematics relating the drag and lateral accelerations to the longitude, latitude, and heading angle and energy (energy being the independent variable). The planning methods presented in this paper are based on these kinematics. An alternative to using this third-order kinematic system is to use the fifth-order system (2). In using the third-order system, we are eliminating the vertical dynamics as represented by the differential equations for r and γ. The potential advantage of eliminating the vertical dynamics is to avoid the relatively fast phugoid-like exchanges between kinetic and potential energy that would make integration of the differential equation system more difficult and sensitive. Although we do not explicitly consider the vertical dynamics, they are implied by variables we do consider. For a given energy and angle of attack, the drag specifies a radial distance r. The first derivative of drag with respect to energy is related to the flight-path angle γ, and the second derivative of drag is related to the longitudinal component of the lift acceleration $L\cos\sigma$. These relations will be used to extract these variables.

It is our purpose in this paper to contribute to the development of this reduced-order approach. Assessing whether or not the reduced-order approach is indeed advantageous relative to the full-order approach is left for future work.

Desirable Control Set

We need to define the desirable set of values of the intermediate controls D and $(L/D)\sin\sigma$. The first step is to express the vehicle constraints as constraints on the drag acceleration.[8] The dynamic pressure, aerodynamic acceleration, and heating-rate constraints take the form

$$D \le q_{\max} S C_D[\alpha, M(E, \hat{r})]$$

$$D \le A_{\max}\left(1 + \left\{\frac{L}{D}[\alpha, M(E, \hat{r})]\right\}^2\right)^{-\frac{1}{2}}$$

$$D \le \dot{Q}_{\max}\frac{C_D[\alpha, M(E, \hat{r})]S}{2mc^2 V^{2(k-1)}} \tag{12}$$

We approximate r by $\hat{r}$ in these constraints. Then at each value of the energy in the range $[E_0, E_f]$, the drag constraints depend only on α. We now describe the process for generating the desirable set of values of the controls $[D, (L/D)\sin\sigma]$ at each value of E. The drag constraints are the only hard constraints that limit the values of the intermediate controls. What we are calling the desirable set is further restricted by requiring that an equilibrium glide condition can be satisfied. An example of the desirable set for a particular value of normalized energy is shown in Fig. 2. Normalized energy is defined as $(E - E_0)/(E_f - E_0)$ such that the initial and final values are 0 and 1, respectively.

For a given value of $\alpha \in [\alpha_{\min}, \alpha_{\max}]$, the maximum drag acceleration $D_{\max}$ is the least upper bound dictated by the three drag constraints. For the same value of α, we compute the L/D. Next we plot the $[D, (L/D)\sin\sigma]$ curve generated by different values of σ according to

$$D = \frac{g - V^2/\hat{r}}{(L/D)\cos\sigma}, \qquad \frac{L}{D}\sin\sigma = \frac{L}{D}(1 - \cos^2\sigma)^{\frac{1}{2}} \tag{13}$$

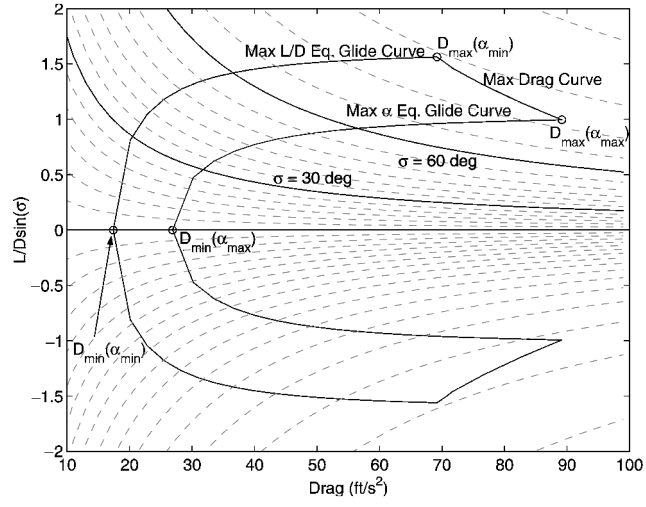

Fig. 2 Desirable control set for a normalized energy of 0.5 and a reusable second-stage vehicle model. Each – – – curve shows the values of $[D, (L/D)\sin\sigma]$ for a fixed σ as α is varied.

The first equation is derived from the level-flight equilibrium glide condition. As earlier, we only consider the subcircular case for which $(g - V^2/r) > 0$. With L/D fixed by the value of α, specifying σ determines the value of D, which balances the lift force with the effective weight $[m(g - V^2/r)]$ and also determines the lateral acceleration $L \sin\sigma$, or equivalently $(L/D)\sin\sigma$. We start with $\sigma = 0$ and work up to the value of σ for which $D = D_{\max}$; larger values of σ are not allowed. The curve for negative values of σ is just the reflection about the D axis of the curve for positive σ. Repeating these calculations, for each value of α the curves of $[D, (L/D)\sin\sigma]$ generate the desirable set for a given energy. Then repeating the preceding process for each energy, the entire desirable set is generated.

In Fig. 2, for a normalized energy of 0.5 we show the maximum L/D equilibrium glide curve (the one corresponding to the value of α that yields the maximum L/D) and the maximum alpha (40-deg) equilibrium glide curve; these two curves define boundaries of the desirable set. The dashed curves are the values of $[D, (L/D)\sin\sigma]$ for a fixed σ as α is varied. Also shown is the maximum drag curve through the points that are the maximum values of drag and the corresponding values of $(L/D)\sin\sigma$ for the range of α values; this curve is also a boundary of the desirable set. In the example, $\alpha_{\min}$ is the α corresponding to $(L/D)_{\max}$. If $\alpha_{\min}$ is less than the value for $(L/D)_{\max}$, then the maximum $(L/D)\sin\sigma$ point on the maximum drag curve would not correspond to $\alpha_{\min}$. The largest desirable set has a boundary on the maximum L/D equilibrium glide curve because the progression of the equilibrium glide curves with α reverses direction at the value of α corresponding to $L/D_{\max}$. This is because in hypersonic entry the vehicle operates on the side of the L/D vs α curve where increasing α decreases L/D.

Being in the desirable set is important because for each pair $[D, (L/D)\sin\sigma]$ in this set there is a corresponding pair (α, σ) such that the drag constraints are satisfied and equilibrium glide flight is possible. If the pair $[D, (L/D)\sin\sigma]$ is in the convex hull of the desirable set, but not in the desirable set, then there exists a corresponding pair (α, σ) such that the drag constraints are satisfied but equilibrium glide is not possible. Transient excursions through this region, such as during a bank reversal, are allowed, but there will be limited capability to track this portion of the trajectory and accommodate dispersions.

Feasible Planning

Within the entry trajectory planning problem two subproblems can be identified (Fig. 1). The trajectory length subproblem (an inverse problem) is as follows: given the trajectory length S, determine a consistent drag profile that meets the drag constraints. The trajectory curvature subproblem is the following: given the drag profile, determine the lateral acceleration profile that minimizes the target error. In terms of these subproblems, the onboard trajectory planning for the shuttle consists of solving only the trajectory length subproblem, under the restrictive assumption that the trajectory has no curvature in the horizontal dimension.

A natural extension of the shuttle method is the following feasible trajectory planning concept:

1) Estimate the trajectory length, and solve the trajectory length subproblem to obtain an initial drag profile.

2) Using the current estimate of the drag profile, solve the trajectory curvature subproblem.

3) Based on the solution to the trajectory curvature subproblem, adjust the trajectory length and resolve the trajectory length subproblem to obtain a revised drag profile.

4) If the target error is sufficiently small, stop; otherwise, repeat steps 2–4.

This successive approximation method generates a feasible trajectory. The first step is the shuttle planning of the drag profile. By including the remaining steps, both drag and lateral acceleration profiles can be planned, and an entry requiring significant trajectory curvature can be handled.

A particular version of feasible trajectory planning has been developed and tested. The method is initialized by specifying an energy-dependent angle-of-attack profile and estimating the required trajectory length as the length of a great circle arc at $\hat{r} = (r_0 + r_f)/2$. The drag profile is represented as a function of energy by three linear spline segments. The endpoints of the profile are fixed to desired initial and final drag values, and the second segment is specified as a constant drag profile. These constraints and continuity requirements specify all but one of the parameters. The drag constraints can be met either by inserting constraint arcs into the drag profile or by introducing additional parameters to move the profile within the constraint boundaries. Using a Newton iteration scheme, the free parameter is determined such that the specified trajectory length is achieved. With the trajectory length subproblem solved in this manner, we proceed to the trajectory curvature subproblem.

The trajectory curvature subproblem is solved by determining the magnitude of $(L/D)\sin(\sigma)$ and then determining the sign of $(L/D)\sin(\sigma)$ by integrating the reduced-order system. The magnitude of $(L/D)\sin(\sigma)$ is determined either by assuming equilibrium glide flight or from knowledge of D''. The latter alternative is the correct approach because, once the drag profile is specified, the vertical component of lift is specified by D'', but the equilibrium glide approach is simpler and may be adequate. With the equilibrium glide assumption and the specified alpha profile the desirable set collapses to a single curve in the $[D, (L/D)\sin\sigma]$ plane, which is symmetric about the D axis. This curve illustrates that the magnitude of $(L/D)\sin(\sigma)$ is a function of D at each energy. Thus, given $D(E)$ we can compute $(L/D)\cos(\sigma)$ and $|(L/D)\sin(\sigma)|$. Alternatively, we can obtain the vertical component of L/D by differentiating the drag acceleration from Eqs. (3) twice with respect to energy, which yields

$$D'' = a + b[(L/D)\cos\sigma] \tag{14}$$

where

$$a = D\left(\frac{C_D''}{C_D} - \frac{C_D'^2}{C_D^2}\right) + D'\left(\frac{C_D'}{C_D} + \frac{2}{V^2}\right) - \frac{4D}{V^4} + \frac{1}{DV^2}\left(\frac{1}{h_s} + \frac{2g}{V^2}\right)\left(g - \frac{V^2}{r}\right)$$

$$b = -\frac{1}{V^2}\left(\frac{1}{h_s} + \frac{2g}{V^2}\right) \tag{15}$$

and $h_s = -\rho(\partial\rho/\partial r)^{-1}$ is the density scale height and then solving for $(L/D)\cos(\sigma)$, which yields

$$(L/D)\cos\sigma = (1/b)(D'' - a) \tag{16}$$

In Eqs. (14) and (15) we have used the approximations $\cos\gamma \cong 1$ and $D + g\sin\gamma \cong D$ and neglected a term proportional to $\sin^2\gamma$. Because D has been determined in the form of a three-segment linear profile, the values for D' and D'' are known to be a constant and 0, respectively, for each segment. For our numerical results we calculate the value of C_D' using a finite difference approximation and assume $C_D'' = 0$. Using the alpha profile and $r = \hat{r}$, $(L/D)\cos\sigma$ and L/D can be computed and then used to compute $|(L/D)\sin\sigma|$ by

$$|(L/D)\sin\sigma| = \{(L/D)^2 - [(L/D)\cos\sigma]^2\}^{\frac{1}{2}} \tag{17}$$

With the values of L/D, $L/D\cos\sigma$, and $|L/D\sin\sigma|$ determined by one of the two methods, all that remains is to specify the sign of $(L/D)\sin\sigma$, or equivalently, the sign of the bank angle σ. The sign of σ at the initial energy is taken to be the sign of $\psi(E_0)$. Then assuming a single bank reversal, modeled as a constant maximum rate change through $\sigma = 0$ to the same bank angle with the opposite sign, the energy at which the bank reversal is initiated is adjusted iteratively using a secant method to minimize the cross-range error at the final energy. The final longitude and latitude are predicted by integration of the reduced-order system.

After the solution to the trajectory curvature subproblem converges to a specified tolerance, a revised trajectory length (S_i) is computed by

$$S_i = S_{i-1} + [S_0 - \hat{r}\theta_{i-1}(E_f)] \tag{18}$$

where S_0 is the initial estimate of the trajectory length based on the great circle arc assumption, the subscript $i = 1, 2, 3 \ldots$ is the iteration index for the trajectory length subproblem, and $[S_0 - \hat{r}\theta_{i-1}(E_f)]$ is the downrange that must be added to reach the target. In the coordinate system we use the correct downrange distance to the target is S_0, and if the correct downrange is achieved in the ith iteration then $\hat{r}\theta_i(E_f) = S_0$. If $|S_i - S_{i-1}|$ is not less than a specified tolerance, then the trajectory length subproblem is resolved using S_i to update the drag profile.

The final desired trajectory is obtained by iterating between the trajectory length and curvature subproblems. The stopping criterion for the iterations is that the final errors in θ and ϕ are within specified tolerances or the solution stops improving. It is of course possible to specify final conditions for which no feasible solution exists. For the specific algorithm we have proposed, the search for the bank reversal energy is the most time consuming because it requires numerical integration. The solution of the curvature subproblem takes between 10 and 15 iterations to converge within 1 n mile; longer trajectories require a number of iterations at the higher end of this range because the bank reversal energy has to be determined more precisely.

This planning method will generate a feasible trajectory that can be used either directly or as a starting solution for the optimal trajectory planner described in the next subsection. At the expense of increased computation, greater flexibility in shaping the trajectory can be achieved by allowing more than one bank reversal and representing the drag profile with more and/or higher-order spline segments. We have used the linear spline to illustrate our method, but expect that this will not be adequate in general. In describing the shuttle guidance algorithm, Harpold and Graves[8] state that "selection of the shape and the number of drag acceleration profile segments is dependent on the vehicle configuration, vehicle constraints, and the type of mission to be flown."

Optimal Planning

Another approach to entry trajectory planning is to pose and solve an appropriate optimal control problem. Relative to the feasible planning approach, optimal planning offers more capability at the price of greater computational complexity and effort. We present a formulation based on the reduced-order system in which the drag and lateral accelerations are considered to be the control variables.

The optimal control problem is as follows: Minimize the performance index

$$J = w_\psi[\psi(E_f) - \psi_f]^2 + \int_{E_0}^{E_f} \left[w_H \frac{V}{\sqrt{D}} + w_{u'}\left(v_1^2 + b_v v_2^2\right) + w_\phi \phi^2 + w_u\left(b_1 F_1^2 + b_2 \frac{1}{F_2} + b_3 F_3\right)\right] \mathrm{d}E \tag{19}$$

subject to the differential constraints Eqs. (11); initial state conditions $x(E_0) = x_0$; the terminal state conditions $\Gamma[x(E_f)] = 0$; and the constraints $|v_1(E)| \le v_{1_{\max}}$ and $|v_2(E)| \le v_{2_{\max}}$, $\forall E \in [E_0, E_f]$, where $x = (\theta, \phi, \psi)$, $u = (u_1, u_2) = [D, (L/D)\sin\sigma]$, and $v = (v_1, v_2)$. Along with the three equations of motion, the two additional differential equations $u_1' = v_1$ and $u_2' = v_2$ are included in the differential constraints. The w and b weighting factors are all nonnegative. The desired final heading angle is specified as a soft constraint. Noting that $V/\sqrt{D}$ is proportional to $\mathrm{d}Q/\mathrm{d}E$, the heat load is included in J if $w_H > 0$. If $w_{u'} > 0$, the rates of change of u_1 and u_2 with respect to energy are penalized. If $w_u > 0$, then the condition that (u_1, u_2) belong to the desirable control set is included as a soft constraint.

The functions F_1, F_2, and F_3 represent the maximum drag, $\alpha_{\max}$ equilibrium glide, and $(L/D)_{\max}$ equilibrium glide constraint curves, the boundaries of the desirable set as shown in Fig. 3. One of these functions is equal to unity when (u_1, u_2) is on the boundary of the desirable set. The equations for F_1, F_2, and F_3 that approximate the boundaries of the desirable set are

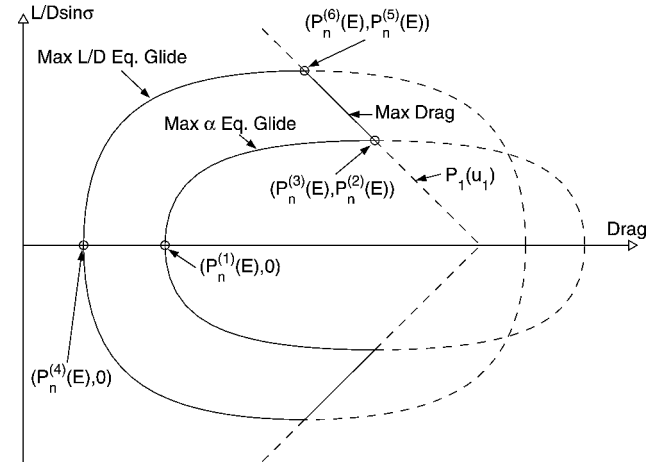

Fig. 3 Approximated boundaries for the desirable set at a particular energy.

$$F_1 = \frac{u_2(E)}{P_1(u_1)}$$

$$F_2 = \left[\frac{u_1(E) - P_n^{(3)}(E)}{P_n^{(1)}(E) - P_n^{(3)}(E)}\right]^4 + \left[\frac{u_1(E) - P_n^{(3)}(E)}{P_n^{(1)}(E) - P_n^{(3)}(E)}\right]^2 + \left[\frac{u_2(E)}{P_n^{(2)}(E)}\right]^2 + \left[\frac{u_2(E)}{P_n^{(2)}(E)}\right]^4$$

$$F_3 = \left[\frac{u_1(E) - P_n^{(6)}(E)}{P_n^{(4)}(E) - P_n^{(6)}(E)}\right]^4 + \left[\frac{u_1(E) - P_n^{(6)}(E)}{P_n^{(4)}(E) - P_n^{(6)}(E)}\right]^2 + \left[\frac{u_2(E)}{P_n^{(5)}(E)}\right]^2 + \left[\frac{u_2(E)}{P_n^{(5)}(E)}\right]^4 \tag{20}$$

where $P_1(u_1)$ is a linear function of u_1 that approximates u_2 along the maximum drag boundary. $P_n^{(1)}(E)$ through $P_n^{(6)}(E)$ are nth-order polynomials in E; they allow the functions F_1, F_2, and F_3 to vary appropriately with energy. $P_n^{(1)}(E)$, $P_n^{(2)}(E)$, and $P_n^{(3)}(E)$ fit the minimum drag, maximum $(L/D)\sin\sigma$ and maximum drag occurring on the maximum alpha boundary. $P_n^{(4)}(E)$, $P_n^{(5)}(E)$, and $P_n^{(6)}(E)$ fit the minimum drag, maximum $(L/D)\sin\sigma$, and maximum drag occurring on the $(L/D)_{\max}$ equilibrium glide boundary. Figure 3 shows how the three-dimensional corridor is approximated by the polynomial fits of $P_n^{(1)} - P_n^{(6)}$ and P_1 as functions of energy. The accuracy of the functions F_2 and F_3 in approximating the boundaries of the desirable set is not vital to the planner because equilibrium glide constraints can be violated for short periods of time. On the other hand, the accuracy of the function F_1 is important because it represents the maximum drag boundary, a physical limitation of the vehicle. To ensure that the inaccuracy of F_1 does not allow for a violation of the drag constraint, the maximum drag limit is reduced slightly from its actual value. For the numerical results presented in this paper, a value of $n = 7$ was used, and the maximum drag limit was reduced by about 5 ft/s^2.

With the desirable set defined by the three approximate boundaries and the various terms in the performance index, a variety of optimal control problems could be posed. Constraints on the desirable set, terminal conditions, and control rates can be enforced as a combination of either hard or soft constraints. Based on our experience, the most effective formulation has hard constraints on the final longitude, final latitude, maximum drag boundary, and control rates and soft constraints on the final heading, the control rates, the $\alpha_{\max}$ and $(L/D)_{\max}$ boundaries, and the maximum drag boundary. Using the type of soft constraints on the desirable set defined in Eq. (20) favors trajectories that are in the interior of the desirable set. Hard constraints on the final longitude and latitude ensure that the trajectory satisfies these terminal conditions accurately. To prevent rapid changes in the drag and lateral accelerations and limit the number of

bank reversals, both hard and soft constraints on the control rates are imposed.

Determining Remaining State and Control Variables

We use a reduced-order model to simplify and reduce the numerical sensitivity of the trajectory planning computations. The reduced-order trajectory planning determines θ, ϕ, ψ, D, and $(L/D)\sin\sigma$ as functions of E. The remaining state and control variables can be determined from this information and the differential equations.

Differentiating the model for the drag acceleration with respect to E and neglecting derivatives of the drag coefficient yields

$$D' = \left(\frac{C_D'}{C_D} + \frac{2}{V^2}\right) D + \left(\frac{1}{h_s} + \frac{2g}{V^2}\right) \sin\gamma \qquad (21)$$

Because $D'(E)$ is known from the planning, there is enough information, using $r(E) = \hat{r}(E)$, to determine $\gamma(E)$. Using a finite difference to approximate $\gamma'(E_0)$, we then have four algebraic equations corresponding to D, $(L/D)\sin\sigma$, D', and γ' from which to extract the values of the four unknowns r, γ, α, and σ at the initial energy E_0. For the feasible planner the α profile is assumed a priori and does not need to be computed. This procedure can be repeated at each energy step, but better results are obtained by applying Euler integration to the r' and γ' differential equations to propagate r and γ from the values computed at E_0. The controls α and σ are computed at each step from the known values of r, D, and $(L/D)\sin\sigma$. The values of r, γ, α, and σ computed in this manner, combined with the values of θ, ϕ, ψ, D, and $(L/D)\sin\sigma$ from either planner, will be referred to as the reference trajectory and controls.

With the controls α and σ determined for the entire range of energy and with the state variables determined at the initial energy, the equations of motion (2) can be integrated to compute the state variables and corresponding values of D and $(L/D)\sin\sigma$ at the other values of energy. The information at the other energy values computed by this open-loop simulation will in general differ from the reference information computed by either the feasible or optimal planner and the extraction procedure just described. To reduce the differences, feedback terms can be added to better track the reference D profile. For the purpose of this paper, simple feedback laws are used: the angle-of-attack and bank angle determined from the algebraic extraction are incremented by

$$\Delta\alpha = k_1 C_D (D_r - D), \qquad \Delta\sigma = \pm[k_2 \Delta\alpha - k_3 (D_r' - D')] \qquad (22)$$

where the sign of $\Delta\sigma$ is taken to be the same as the sign of σ. We will refer to the simulation with the controls incremented in this manner as the closed-loop simulation.

Results and Discussion

Results for the feasible and optimal planners are presented for the purpose of illustrating their capabilities. A detailed analysis and performance assessment is beyond the scope of this paper.

Feasible Planning

The feasible planning algorithm was coded and tested in the MATLAB® environment using an X-33 vehicle model.[1] According to the model, the X-33 has a weight of 83,000 lb, reference area of 1608 ft^2, maximum C_L of 0.8, and maximum L/D of 3.7 at an angle of attack of 11 deg. Figures 4 and 5 shows a solution from the planner for boundary conditions corresponding to a baseline Michael 10a1 trajectory.[17] Michael 10a1 is a suborbital trajectory designed for the X-33 program to yield the least aerodynamic and thermal loads. The descent phase of the trajectory begins at a position of $-116.15°$ longitude and 36.59° latitude and ends at TAEM interface conditions appropriate for landing at Michael Army Air Field. The TAEM interface position is $-112.95°$ longitude and 40.22° latitude. The initial heading is 35.04° from north. These angles are transformed to the target coordinate frame. The initial and final altitudes ($h = r - r_s$) and velocities for the 10a1 trajectory are $h_0 = 1.727 \times 10^{+5}$ ft, $h_f = 9.6 \times 10^{+4}$ ft, $V_0 = 9501.297$ ft/s, and $V_f = 3000$ ft/s. The constraints on normal acceleration, dynamic pressure, and maximum angle of attack are $q_{\max} = 400$ lb/ft^2, $A_{\max} = 80.5$ ft/s^2, $\alpha_{\max} = 40$ deg, and $\alpha_{\min} = \alpha$ for $(L/D)_{\max}$. The tolerances for determining convergence were 1 n mile error in downrange and 0.35 n mile error in crossrange. The planner achieved a final error of 0.3 n mile from the desired target. The computed drag profile is shown in Fig. 4 and remains within the drag constraints. The assumed α profile and the computed σ profile are plotted in Fig. 5. A finite bank reversal maneuver with $|\dot{\sigma}| = 5$ deg/s was used. The required $|\dot{\sigma}|$ is less than 5 deg/s everywhere else.

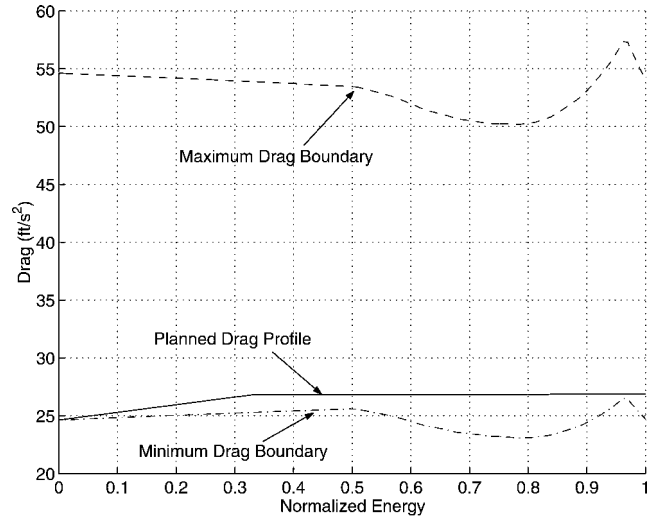

Fig. 4 Drag profile from feasible planner.

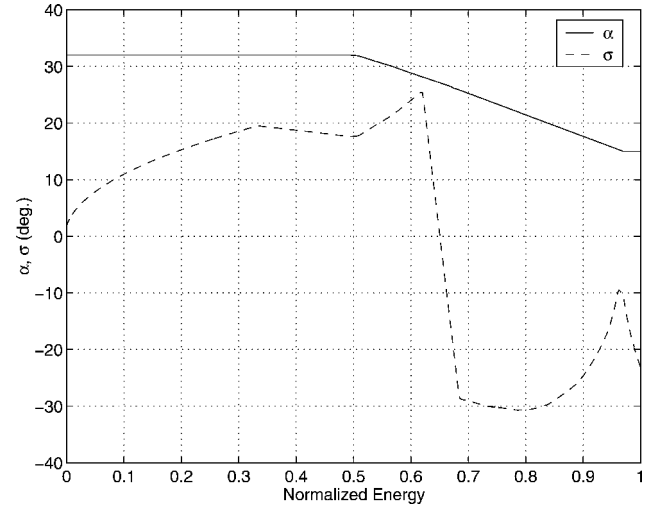

Fig. 5 σ profile from feasible planner and assumed α profile.

Optimal Planning

As a first step in assessing the efficacy of the optimal planning approach, we present and discuss results obtained by solving the optimal control problem with a general purpose optimization code: the Sparse Optimal Control Software (SOCS).[18] SOCS solves the optimal control problem using a direct transcription method. The state and control variables are discretized to cast the optimal control problem as a nonlinear programming problem. The solution to the sparse nonlinear programming problem is then determined using sequential quadratic programming. We envision that a special purpose optimization algorithm would be used for the onboard implementation of our approach for faster computation and reduced code size and complexity. For onboard, real-time implementation, the desirable set could be characterized in a simpler manner than already stated. In any case the characterization of the desirable set is done in the design of the guidance algorithm and is then a fixed part of the algorithm, unless there are changes to the vehicle constraints.

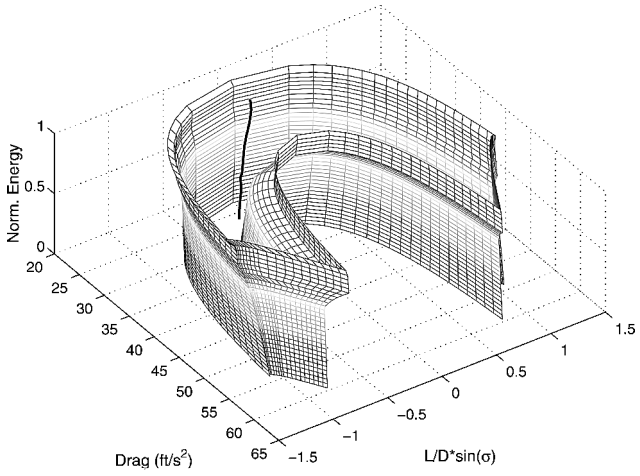

Fig. 6 Intermediate control trajectory within desirable set (boundaries of set shown).

The optimal planning algorithm was applied to the X-33 model and the same baseline boundary conditions for the Michael 10a1 trajectory. The reference radius as a function of energy and initial guesses for the drag and lateral acceleration profiles were obtained through linear interpolation between the initial and final values. The weighting factors for the performance index [Eq. (19)] were $w_\psi = 0$, $w_H = 5.55 \times 10^{-4}$, $w_\phi = 0$, $w_{u'} = 5 \times 10^{-6}$, $w_u = 0.2$, $b_v = 500$, $b_1 = 0.3$, $b_2 = 3.5$, and $b_3 = 0.7$. Figure 6 shows the desirable set of intermediate controls and the computed optimal solution. The solution lies within the desirable set.

The integral penalty on ϕ limits the lateral excursions from a "straight" path to the target, i.e., from a trajectory with $\phi \equiv 0$. As the weighting factor w_ϕ is increased, the number of bank reversals increases while the maximum lateral excursion decreases. Trajectories obtained from the planner with and without a penalty on ϕ are shown in Fig. 7. The weighting factors for the performance index are the same as already stated except that $w_{u'} = 1 \times 10^{-6}$. The initial and final altitudes and velocities are $h_0 = 1.727 \times 10^{+5}$ ft, $h_f = 9.6 \times 10^{+4}$ ft, $V_0 = 12001.297$ ft/s, and $V_f = 3000$ ft/s. The initial heading angle is 85 deg; the initial longitude and latitude are both

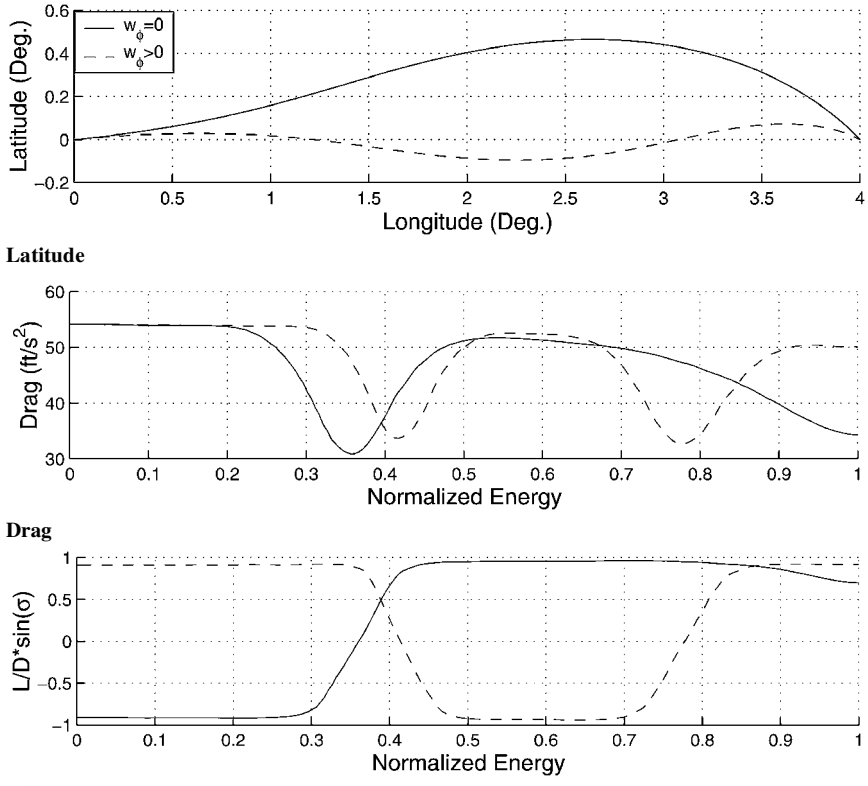

Fig. 7 Optimal trajectories with and without penalty on ϕ.

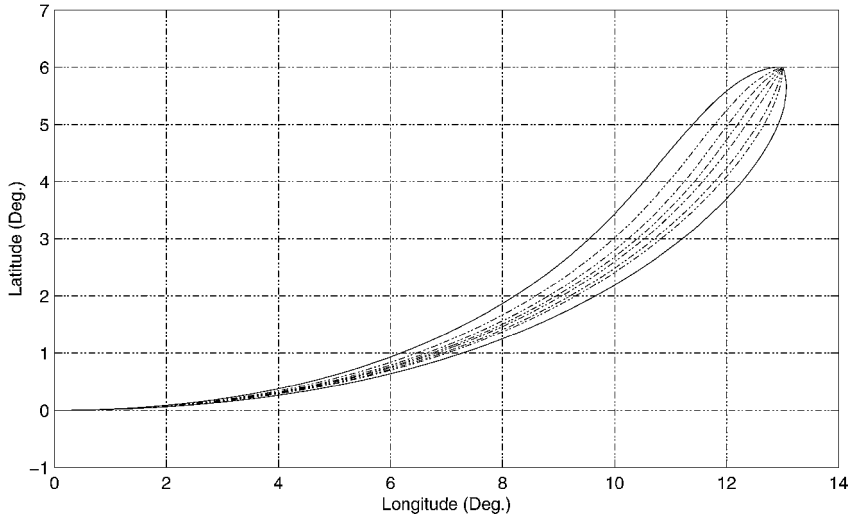

Fig. 8 Long-range trajectories for various final heading angles.

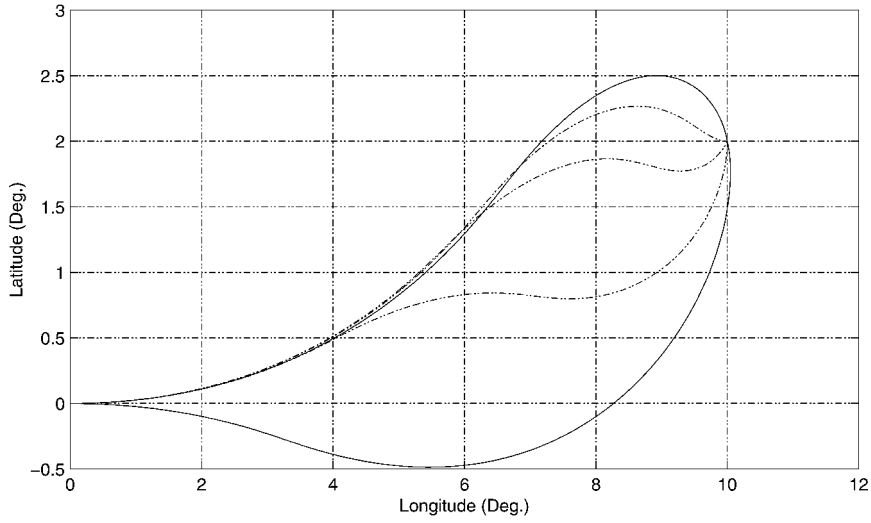

Fig. 9 Short-range trajectories for various final heading angles.

0°; and the final longitude and latitude are 4° and 0°, respectively. In comparison to $w_\phi = 0.0$, a weighting factor of $w_\phi = 0.7$ reduces the maximum lateral excursion from 0.5 to 0.1 deg by introducing a second bank reversal. We note that the maximum lateral excursion varies continuously with w_ϕ, whereas the number of bank reversals is a piecewise constant function of w_ϕ. It is thus possible to vary the maximum lateral excursion to some extent for a fixed number of bank reversals by adjusting w_ϕ.

If the available energy is greater than the minimum required to achieve the specified longitude and latitude, a range of final heading angles can be reached. It may then be desirable to achieve a particular final heading angle within this range, e.g., to align the vehicle with the runway. With the two-dimensional shuttle planner it is not possible to specify the final heading angle; with the optimal three-dimensional planner it is. A reusable second stage vehicle model supplied by Boeing is used to generate results illustrating this feature. The reusable second stage has a weight of 85,000 lb; reference area of 1300 ft^2; maximum C_L of 3.6; and a maximum L/D of 8.0 at an angle of attack of 10 deg. Figure 8 shows several trajectories generated under identical conditions, except that different final heading angles are specified via a penalty term in the cost function. For this entry problem the feasible final heading angles range from −20 to 90 deg. With a shorter downrange requirement a larger range of final heading angles is reachable, −20 to 160 deg, because there is more energy available for turning. Several trajectories spanning this range of final heading angles are shown in Fig. 9.

Extraction

Once a solution is obtained by either the feasible or the optimal reduced-order planner, the remaining state and control variables can be extracted. The extraction algorithm, described in the preceding section, was applied to the reduced-order solution from the optimal planner shown in Fig. 6. Data from the computed reference trajectory were then used, as described earlier, to drive open-loop and closed-loop simulations. For the closed-loop simulation the gains in Eqs. (22) were set to $k_1 = 1, k_2 = 0.05$, and $k_3 = 0$. The reference, open-loop, and closed-loop altitude, flight-path angle, angle of attack, bank angle, and drag are compared in Figs. 10 and 11. The open-loop α and σ are not shown because they are by definition the same as the reference values. The altitude and flight-path angle do not differ much between the three cases. The closed-loop angle of attack differs by a maximum value of 3 deg from the reference angle of attack, whereas the closed-loop bank angle differs only slightly from the reference bank angle. Relative to the reference longitude and latitude at the final energy, the maximum error when translated to distance on the ground is 2.7 n miles for the open-loop case and 0.16 n mile for the closed-loop case. Figure 11 shows that the closed-loop simulation tracks the reference D more closely than the drag

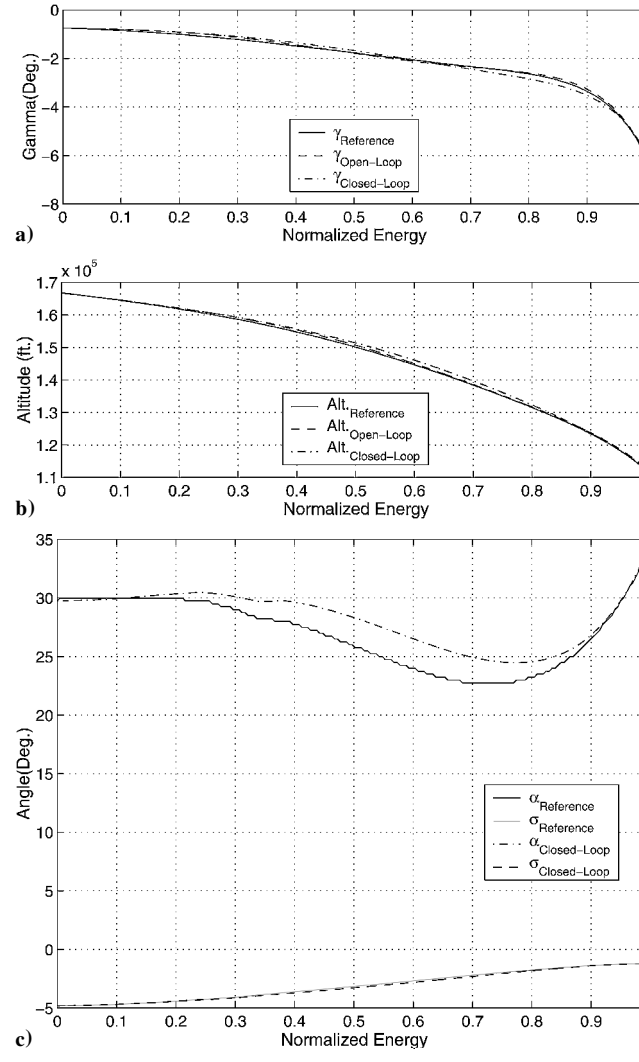

Fig. 10 Extracted state and control variables as functions of normalized energy a) γ, b) altitude, and c) α and σ.

acceleration from the open-loop simulation. The jaggedness of the open-loop drag acceleration is caused by the use of aerodynamic look-up tables in the extraction algorithm. Compared to the differences in the drag acceleration, the lateral acceleration differences are much smaller for the three cases.

The closed-loop trajectory and controls could be used as a revised reference. Because the state and control variables satisfy the equations of motion, it should be easier to track.

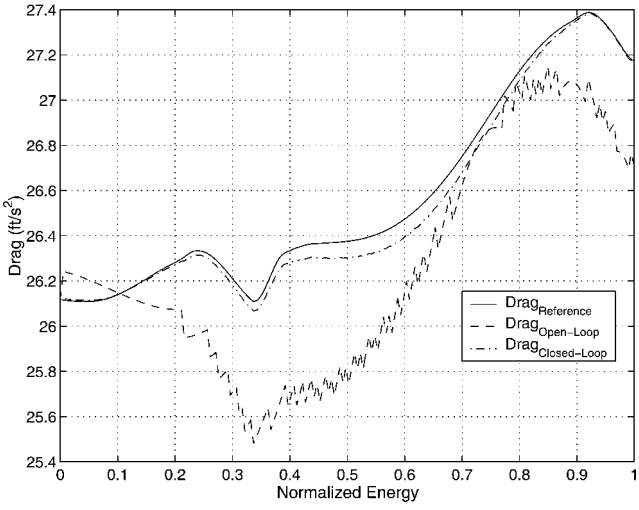

Fig. 11 Comparison of reference, open-loop, and closed-loop drag accelerations.

Conclusions

Three differential equations that are the kinematic relations between the aerodynamic accelerations and the position and velocity variables with energy as the independent variable have been used as the basis for two methods of planning the drag and lateral acceleration profiles for an entry trajectory. The first method produces a feasible trajectory for a given angle-of-attack profile. It is a direct extension of the drag acceleration planning method used for the shuttle and can accommodate large cross-range entry because it accounts for the lateral curvature of the trajectory. The second method requires more computation, but produces an optimal trajectory assuming that the drag and lateral accelerations can be independently adjusted within limits via angle-of-attack and angle-of-bank variations. The second method has greater capability to shape the entry trajectory. The methods have been demonstrated using an X-33 vehicle model. The optimal method is capable of achieving a specified final heading angle and adjusting the number of bank reversals.

Acknowledgments

Support for this research was provided by McDonnell Douglas, Boeing, and the NASA Marshall Space Flight Center (MSFC); the authors specially thank D. Young and S. Tandon (McDonnell Douglas, Boeing) and J. Hanson (MSFC). The second author was supported in part by a Holmes fellowship. Discussions with C. Graves of the NASA Johnson Space Center have contributed significantly to the first author's understanding of the shuttle entry guidance. Comments from Associate Editor P. Lu and two anonymous reviewers led to improvements in the paper.

References

[1]Hanson, J. M., Coughlin, D. J., Dukeman, G. A., Mulqueen, J. A., and McCarter, J. W., "Ascent, Transition, Entry, and Abort Guidance Algorithm Design for the X-33 Vehicle," AIAA Paper 98-4409, Aug. 1998.

[2]Stengel, R. F., "Optimal Guidance for the Space Shuttle Transition," *Journal of Spacecraft and Rockets*, Vol. 11, No. 3, 1974, pp. 173–179.

[3]Lu, P., "Regulation About Time-Varying Trajectories: Precision Entry Guidance Illustrated," *Journal of Guidance, Control, and Dynamics*, Vol. 22, No. 6, 1999, pp. 784–790.

[4]Powell, R. W., "6-Degree-of-Freedom Guidance and Control-Entry Analysis of the HL-20," *Journal of Spacecraft and Rockets*, Vol. 30, No. 5, 1993, pp. 537–542.

[5]Fuhry, D. P., "Adaptive Atmospheric Reentry Guidance for the Kistler K-1 Orbital Vehicle," *Proceedings of the Guidance, Navigation, and Control Conference*, AIAA, Reston, VA, 1999, pp. 1275–1288.

[6]Chou, H.-C., Ardema, M. D., and Bowles, J. V., "Near-Optimal Entry Trajectories for Reusable Launch Vehicles," *Journal of Guidance, Control, and Dynamics*, Vol. 21, No. 6, 1998, pp. 983–990.

[7]Bryson, A. E., Jr., Carroll, F. J., Zvara, J., Black, A., Blatt, P., Bohling, R., Burke, M., Kanter, J., Lickly, D., Morth, R., Rosamond, D., and Wingrove, R., "Guidance and Navigation for Entry Vehicles," NASA SP-8015, Nov. 1968.

[8]Harpold, J. D., and Graves, C. A., Jr., "Shuttle Entry Guidance," *Journal of Astronautical Sciences*, Vol. 27, No. 3, 1979, pp. 239–268.

[9]Wingrove, R. C., "Survey of Atmosphere Re-Entry Guidance and Control Methods," *AIAA Journal*, Vol. 1, No. 9, 1963, pp. 2019–2029.

[10]Roenneke, A. J., and Cornwell, P. J., "Trajectory Control for a Low-Lift Re-Entry Vehicle," *Journal of Guidance, Control, and Dynamics*, Vol. 16, No. 5, 1993, pp. 927–933.

[11]Mease, K. D., and Kremer, J.-P., "Shuttle Entry Guidance Revisited Using Nonlinear Geometric Methods," *Journal of Guidance, Control, and Dynamics*, Vol. 17, No. 6, 1994, pp. 1350–1356.

[12]Roenneke, A. J., and Markl, A., "Re-Entry Control to a Drag-vs-Energy Profile," *Journal of Guidance, Control, and Dynamics*, Vol. 17, No. 5, 1994, pp. 916–920.

[13]Lu, P., "Entry Guidance and Trajectory Control for Reusable Launch Vehicle," *Journal of Guidance, Control, and Dynamics*, Vol. 20, No. 1, 1997, pp. 143–149.

[14]Lu, P., and Hanson, J., "Entry Guidance for the X-33 Vehicle," *Journal of Spacecraft and Rockets*, Vol. 35, No. 3, 1998, pp. 342–349.

[15]Jouhaud, F., "Closed Loop Reentry Guidance Law of a Space Plane: Application to Hermes," *Acta Astronautica*, Vol. 26, No. 8–10, 1992, pp. 577–585.

[16]Vinh, N. X., *Optimal Trajectories in Atmospheric Flight*, Elsevier, New York, 1981, pp. 47–62.

[17]Hill, A. D., Anderson, D. M., Coughlin, D. J., and Chowdhry, R. S., "X-33 Trajectory Optimization and Design," AIAA Paper 98-4408, Aug. 1998.

[18]Betts, J. T., and Huffman, W. P., *Sparse Optimal Control Software*, The Boeing Co., Seattle, WA, 1997, Secs. 1-1–2-5.